

Effects of ^3He Impurity on Solid ^4He Studied by Compound Torsional Oscillator

P. Gumann,* M.C. Keiderling, D. Ruffner, and H. Kojima
Serin Physics Laboratory, Rutgers University, Piscataway, NJ 08854 USA

Frequency shifts and dissipations of a compound torsional oscillator induced by solid ^4He samples containing ^3He impurity concentrations ($x_3 = 0.3, 3, 6, 12$ and 25 in units of 10^{-6}) have been measured at two resonant mode frequencies ($f_1 = 493$ and $f_2 = 1164$ Hz) at temperatures (T) between 0.02 and 1.1 K. The fractional frequency shifts of the f_1 mode were much smaller than those of the f_2 mode. The observed frequency shifts continued to decrease as T was increased above 0.3 K, and the conventional non-classical rotation inertia fraction was not well defined in all samples with $x_3 \geq 3$ ppm. Temperatures where peaks in dissipation of the f_2 mode occurred were higher than those of the f_1 mode in all samples. The peak dissipation magnitudes of the f_1 mode was greater than those of the f_2 mode in all samples. The activation energy and the characteristic time (τ_0) were extracted for each sample from an Arrhenius plot between mode frequencies and inverse peak temperatures. The average activation energy among all samples was 430 mK, and τ_0 ranged from 2×10^{-7} s to 5×10^{-5} s in samples with $x_3 = 0.3$ to 25 ppm. The characteristic time increased in proportion to $x_3^{2/3}$. Observed temperature dependence of dissipation were consistent with those expected from a simple Debye relaxation model *if* the dissipation peak magnitude was separately adjusted for each mode. Observed frequency shifts were greater than those expected from the model. The discrepancies between the observed and the model frequency shifts increased at the higher frequency mode.

PACS numbers: 67.80.-s

I. INTRODUCTION

The discovery¹ that the resonant frequencies of torsional oscillators (TOs) containing solid ^4He samples increased at temperatures below about 300 mK has stirred much excitement (see reviews²⁻⁴). Interpreted as a partial decoupling or so-called⁵ “non-classical rotational inertia (NCRI)” of the solid ^4He samples, the discovery gave evidence for the long-sought⁶ supersolid state of solid ^4He possessing simultaneously crystallinity and superfluid properties. In the temperature range where the observed TO frequency shifts vary most rapidly, peaks in the energy dissipations of the TO are also observed. The frequency shifts and the accompanying dissipations of TO have been confirmed in many laboratories.⁷⁻¹¹ However, the interpretation in terms of supersolid state in the loaded solid ^4He samples remains controversial and a comprehensive understanding of the TO frequency shifts and other related phenomena in quantum solid ^4He at low temperatures has not been established.

There are puzzling observations in experiments designed to test the supersolid interpretation. Superflows that would be expected to occur through supersolid ^4He samples under applied pressure gradients have not been observed in the earlier flow experiments¹²⁻¹⁴ carried out in the same temperature range as the NCRI effect is observed. Recently, however, unusual mass flows^{15,16} were induced through solid ^4He samples below about 0.6 K by applying chemical potential gradients across the samples. Propagation of fourth sound that would be expected^{17,18} for a superfluid has not been detected.^{19,20} The shear modulus of a thin solid ^4He slab was found¹³ to “stiffen” in a very similar manner as the frequency of TO containing an annular solid ^4He sample was found¹ to increase

with decreasing temperature. This similarity indicated a common origin of these two effects. While almost none of these observations are clearly understood, it has become apparent that the details of the observations are affected strongly by the solid ^4He sample quality depending on growth condition, sample geometry and size, and ^3He impurity. The objective of the present work is to gain understanding of the puzzling role played by ^3He impurity by use of our compound TO techniques.

The surprisingly high sensitivity of observed frequency shifts to minute ^3He impurity concentrations (x_3) at parts per million (ppm) levels in the ^4He samples has been reported by Kim, et al.^{1,21} The temperature dependence of the shear modulus was also found¹³ to depend on x_3 . On the other hand, a thermodynamic anomaly in heat capacity occurs at temperatures which are relatively insensitive to the value of x_3 . The dynamics of ^3He atoms within solid ^4He may be probed by NMR experiments. Simultaneous observations of NMR and TO effects, of the same crystal, have been carried out by Toda, et al.^{22,23} in solid ^4He samples with x_3 down to 10 ppm. They found three different spin-lattice relaxation times suggesting the existence of three different states of ^3He atoms in the solid matrix of ^4He . Kim, et al.^{24,25} reported their measurements of NMR relaxation times, T_1 and T_2 , of ^3He contained in solid ^4He samples with x_3 down to 16 ppm. The relation between all of these NMR observations and the role of ^3He impurity in the supersolid phenomenon is yet to be clarified.

One goal of our work is to measure how the dissipations accompanying frequency shifts of solid- ^4He -loaded TO depend on the amount of added ^3He impurity. The earlier reports^{1,21} focused mainly on the variation of frequency shifts as x_3 was changed. Another goal is to measure

how the dependence of frequency shifts and dissipations on the TO frequency varies as x_3 is changed. Frequency dependence studies are difficult in single resonance mode TOs. We report on the first systematic measurements of the dependence of dissipations and frequency shifts on x_3 ($0.3 \sim 25$ ppm) using our compound TO having two resonance mode frequencies (~ 500 and ~ 1200 Hz). Unlike in the earlier ^3He impurity dependence study²¹, all samples are grown in the same torsional oscillator following nearly identical solid growth procedures such that variance due to sample cell geometry and sample quality would be minimized. Measurements are made simultaneously at the two frequencies under identical sample conditions and they allow us to explore dynamical effects which cannot be probed in a single mode TO. For a given sample, the maximum in dissipation of the higher frequency mode appears at a higher (peak) temperature than the lower frequency mode. As x_3 is increased, the peak temperatures for both modes increase. Arrhenius plots of the mode frequencies vs. inverse peak temperatures are analyzed to extract the activation energy and the characteristic time involved in the dissipation process. A simple form of Debye dissipation combined with the extracted characteristic time is inadequate to represent the observed frequency dependent dissipations of the two modes separately. The frequency shifts expected from the dissipation by the Kramers-Kronig relation cannot account for those observed in the two modes. The limiting characteristic time τ_0 extracted from the two modes varies in proportion to $x_3^{2/3}$.

II. EXPERIMENT

Our compound torsional oscillator shown in Fig. 1 was modified from the earlier one^{10,26} and has two torsion rods (a, b) each with diameter 1.9 mm and length 15 mm, and two interconnected masses. The flange above the upper rod (a) is rigidly attached to a large copper vibration isolation block in good thermal contact with the mixing chamber of a dilution refrigerator. The upper mass is a "dummy" comprised of a central disc (c) and two electrode fins (d) made of aluminum plates. The TO is capacitively driven by applying dc-biased sinusoidal voltage between a stationary electrode (not shown) and one of the movable electrode fins. The motion of the TO is detected by measuring the voltage induced between the other electrode fin biased against another stationary electrode (not shown). The lower fin (e) acts as an auxiliary electrode for measuring the motion of the sample chamber itself. The lower mass (f) is mostly made of Stycast 1266 epoxy²⁷ cast around the base (g) below the lower torsion rod. The sample chamber (h) for solid ^4He is an annular space (8.0 mm inner diameter, 10.0 mm outer diameter and 8.0 mm height). Helium is introduced into the chamber via the fill hole (i) drilled (diameter = 0.8 mm) through the center of torsion rods and the base, and a diametrical channel just below the lower surface of

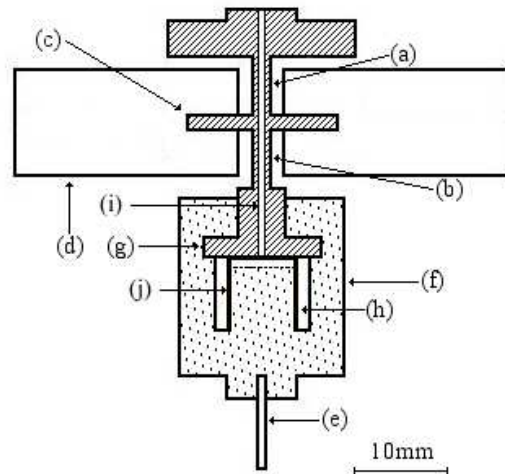


FIG. 1. Schematic of compound torsional oscillator. (a) upper torsion rod, (b) lower torsion rod, (c) upper disc, (d) electrode fins, (e) lower electrode fin, (f) cell body, (g) base, (h) annular sample chamber, (i) fill hole, (j) copper foil liner. The shaded region is machined from a single block of BeCu. The width of the annular sample space is 1.0 mm but shown exaggerated for clarity.

the base. To improve the thermal contact between the sample helium and the mixing chamber, the lower surface of the BeCu base is pressed against a $100\ \mu\text{m}$ thick copper foil (j) which is extended onto the inner wall of the sample space.

The ^3He impurity concentration is increased by adding a calibrated amount of ^3He gas into the cell prior to loading it with the commercial ultra high purity ^4He (nominal $x_3 = 0.3$ ppm) at 4.2 K to approximately 80 bar. A solid sample is subsequently grown by the blocked capillary method. The solid plug formed in the rapidly cooled portion of the filling capillary maintains a constant mass in the sample space below the plug. A Straty-Adams capacitive pressure sensor attached to the isolation block is used to monitor the pressure in the fill tube during sample solid formation. The measured freezing temperature where a sudden increase in the oscillation amplitude occurs gives the pressure in the solid formed. After the plug is formed, the total time elapsed to freeze ^4He in the sample chamber is about 40 minutes for all the samples reported here. Since the sample solid pressure is 40 bar or greater, where the freezing temperature is higher than the highest superfluid ^4He transition temperature, redistribution of ^3He by the heat flush effect is expected to be unimportant. Upon completion of measurements for a given sample, the dilution refrigerator system is warmed up to near 6 K for pumping out helium from the cell. The pressure and the TO resonant frequencies are monitored during this "bake out" procedure to ensure that the remaining residual amount of helium gas is sufficiently small. Subsequent to this procedure, an-

other calibrated amount of ^3He is added such that the ^3He impurity concentration is larger than the previous sample and the above procedure is repeated to grow the next solid sample. In all, measurements were made on solid ^4He samples with $x_3 = 0.3, 3, 6, 12$ and 25 ppm. The samples are identified by their ^3He impurity concentrations. The uncertainty in x_3 is estimated to be $\pm 20\%$.

Sample temperature (T) is inferred from a ruthenium oxide resistance thermometer attached to the isolation block and is calibrated against a ^3He melting pressure thermometer. Reproducibility of the ruthenium oxide thermometer upon cycling up to room temperature is verified with a fixed point superconducting standard down to 15 mK.

The two modes of the compound TO may be excited and detected simultaneously. The resonant frequency and the amplitude of each mode are tracked continuously and independently by two automatic phase-lock feedback data acquisition systems. In all of the data presented in this report, measurements of both modes are taken simultaneously to ensure identical sample conditions. The drive levels are set such that sample velocity amplitude of each mode is less than about $15\text{ }\mu\text{m/s}$. It has been found that effects of "critical velocity" and hysteretic behavior are small at these low velocity amplitudes. The shifts in frequency and amplitudes of the modes can strongly affect each other if the drive levels are increased beyond some threshold velocity.²⁸

Prior to loading the cell with a sample solid, the "background" characteristics of the TO with no helium in the sample chamber are measured during slow (~ 15 mK/hr) cooling and verified for reproducibility by following the temperature dependence of the resonant frequencies, $f_{ib}(T)$, and the oscillation amplitudes, $A_{ib}(T)$, of both modes ($i = 1, 2$). The background quality factor, $Q_{ib}(T)$, is computed from the tracked oscillation amplitude via $Q_{ib}(T) = (A_{ib}(T)/A_{ib}(T_b))Q_{ib}(T_b)$, where the reference quality factor $Q_{ib}(T_b)$ is determined from measured exponential ring down time (reproducible within 10%) at $T_b \approx 200$ mK.

Background characteristics measured at $T = 30$ mK are: $f_{1b} = 493$ Hz, $f_{2b} = 1164$ Hz, $Q_{1b} \sim 7.7 \times 10^5$ and $Q_{2b} \sim 4.7 \times 10^5$. The observed background frequencies are in agreement within $\sim 12\%$ with those computed from estimated moments of inertia and torsion constant of the rods.

After a sample of solid ^4He is grown as described above, the resonant frequencies decrease owing to the added moment of inertia. "Loading frequency" Δf_i^0 in the "zero" temperature limit is defined as $\Delta f_i^0 \equiv f_{ib} - f_{is}$ corresponding to the decrease in the mode frequency from the background to sample-filled cell measured near 30 mK. The measured values are $\Delta f_1^0 = 0.40$ Hz and $\Delta f_2^0 = 1.20$ Hz for the $x_3 = 0.3$ ppm sample shown in Fig. 2. These values are within 10% of those estimated from the added inertia of solid ^4He in the sample chamber. The variation in Δf_i^0 from sample to sample is less than 3% .

After a solid ^4He sample is grown in the cell, the same procedure as in the background characterization including the drive levels is followed to measure $f_{is}(T)$, $A_{is}(T)$, $Q_{is}(T_b)$ and $Q_{is}(T)$. The sample is warmed up at most to 300 mK in the $x_3 = 0.3$ ppm sample, to 1.1 K in the $3, 6$ and 12 ppm samples, and to 2.0 K in the 25 ppm sample. Each sample data set is taken over about 24 hour period while cooling down to ~ 20 mK from 250 mK in the 0.3 ppm sample and from 1 K in all other samples. The measured temperature dependence of $f_{is}(T)$ and $A_{is}(T)$ does not vary significantly from one temperature sweep to another if the maximum temperature is within these limits.

III. RESULTS

A. frequency shift

Our results on frequency shifts are presented in Fig. 2 as "reduced frequency shifts" defined for each mode i as:

$$\delta f_i(T)/f_{is}^0 \equiv \frac{[(f_{ib}(T) - \Delta f_i^0) - f_{is}(T)]}{f_{is}^0}, \quad (1)$$

where f_{is}^0 is the frequency of loaded TO at our minimum temperature (about 15 mK) depending on x_3 . In the zero temperature limit the reduced frequency shift vanishes by definition. It remains, in all samples, at the zero temperature limit below about 40 mK and its magnitude monotonically increases at higher temperatures for both modes. Except in the $x_3 = 0.3$ ppm sample, temperature dependence of the reduced frequency shift of the first mode coincides with that of the second mode below about 100 mK. At temperatures greater than 100 mK changes in reduced frequency of the second mode are greater than those of the first mode. In all samples, except possibly the 0.3 ppm sample, the reduced frequency shifts for both modes continue to decrease as temperature is increased above 200 mK. The lack of data in the 0.3 ppm sample prevents us from making a firm statement about the temperature dependence of the reduced frequency shift above 200 mK in this sample.

The temperature range $50\text{ mK} \lesssim T \lesssim 150\text{ mK}$ where relatively rapid changes in the reduced frequency shift occurs in Fig. 2 has been identified as a signature of the occurrence of NCRI phenomenon. The reduced frequency shifts would become constant if the observed temperature dependence of $f_{is}(T)$ matched that of $f_{ib}(T)$ at temperatures greater than some "onset" temperature where the fraction of solid sample apparently decoupled from the container, or NCRI fraction (NCRI_f), vanishes. Since identifying such onset temperatures in our samples is ambiguous, reduced frequency shifts rather than NCRI_f are shown in Fig. 2.

The reduced frequency shift in the 25 ppm sample shows qualitatively distinct behavior from other samples. In comparison to other samples, there is no temperature

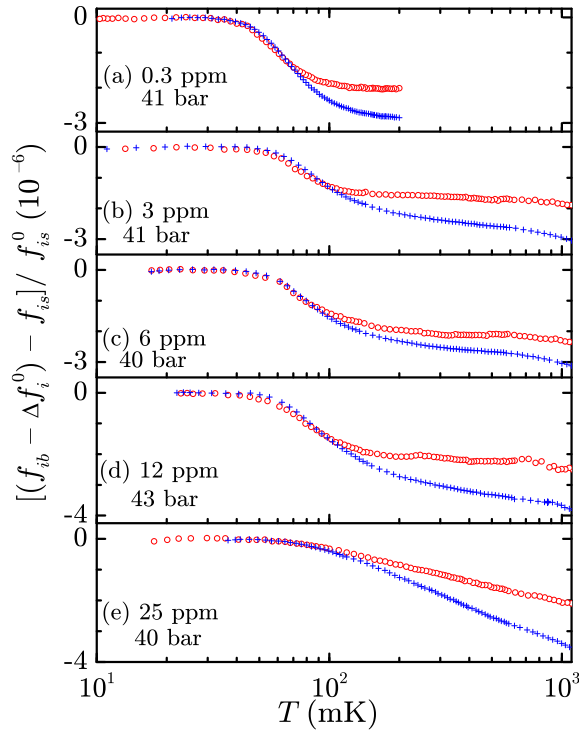


FIG. 2. (color online) Temperature dependence of reduced frequency shift of the compound torsional oscillator with annular sample chamber: first mode ((red) open circles) and second mode ((blue) pluses). Panels (a) ~ (e) show results of solid ^4He samples containing ^3He impurity concentration of 0.3, 3, 6, 12 and 25 ppm, respectively. Indicated solid pressures are estimated from the loading liquid pressure at 4.2 K.

range where the reduced frequency shifts vary relatively more rapidly. At temperatures roughly above 150 mK the frequency shifts decrease linearly (on the logarithmic temperature scale) with the second mode having larger slope than the first. Measured dissipation in the 25 ppm sample is also distinct from other samples (see Fig. 3).

B. dissipation

The change in dissipation of each mode produced by loading solid ^4He samples is computed by taking the difference:

$$\Delta Q_i^{-1}(T) = Q_{is}^{-1}(T) - Q_{ib}^{-1}(T). \quad (2)$$

Evaluated temperature dependence of $\Delta Q_i^{-1}(T)$ is displayed in Fig. 3 for each sample shown in Fig. 2. Samples with $x_3 \leq 12$ ppm have similar temperature dependence with $\Delta Q_i^{-1}(T)$ passing through local maxima at “peak temperatures” (T_{ip}) indicated by arrows in Fig. 3. The 25 ppm sample shows broader temperature dependence than the other samples. The change in dissipation of the first mode is greater than that of the second in all samples. This is in contrast to the reduced frequency shift of

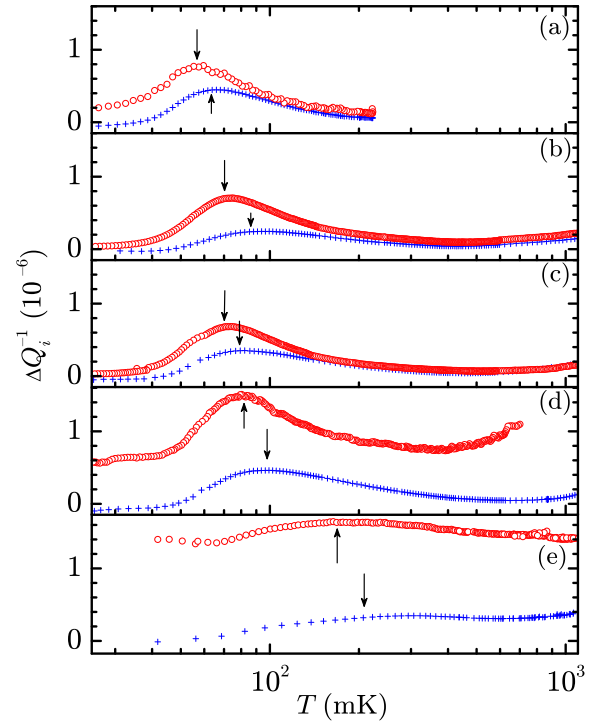


FIG. 3. (color online) Temperature dependence of the change in dissipation from empty to loaded sample chamber: first mode ((red) open circles) and second mode ((blue) pluses). Measurements are taken simultaneously with those reduced frequency shifts in the samples (with the same panel designations for ^3He impurity concentration) as shown in Fig. 2. Arrows indicate temperatures where peaks in dissipation occur.

the second mode being greater than that of the first in all samples at temperatures above 100 mK (see Fig. 2). At temperatures below 40 mK, ΔQ_2^{-1} for some samples is negative. This peculiar feature may have resulted in part from an uncertainty ($\sim 10\%$) in the measurements of reference quality factors and from small inaccuracy in the cell temperature measurement below 40 mK. Small temperature gradients between the sample and the thermometer could lead to errors in taking the difference between the two measurements with the sample chamber being empty and loaded.

The observed frequency dependent peak temperature that the compound TO technique uniquely yields is an important parameter in considering the dynamical effects occurring in the oscillating ^4He samples. The peak temperatures are fairly well-defined except in the 6 and 25 ppm samples whose ΔQ_2^{-1} are broader than the others. The inverse of the peak temperature of the two modes in each sample is shown in Fig. 4. It can be seen that $T_{p2} > T_{p1}$ in all samples. This frequency dependence of the peak temperature was also found in a cylindrical sample chamber geometry in solid ^4He with nominal 0.3 ppm ^3He concentration¹⁰ and appears to be independent of sample geometry and size (down to 0.2 mm), ^3He

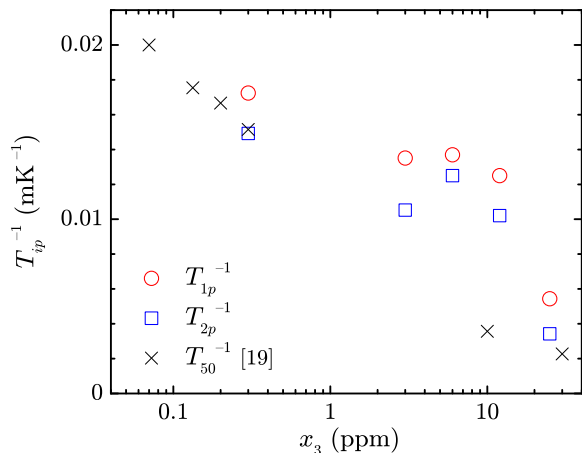


FIG. 4. (color online) Inverse of dissipation peak temperature vs. ^3He impurity concentration: first mode ((red) circles) and second mode ((blue) squares). "Half-maximum temperatures" or T_{50} , (crosses) are taken from Kim, et al.²¹

concentration and sample growth conditions. The peak temperature generally increases for both modes as x_3 is increased. An apparent plateau in T_{ip} in the range $3 \text{ ppm} < x_3 < 10 \text{ ppm}$ is likely caused by some accidental variation in as yet unidentified source of dissipation in the sample characteristics. It is interesting to note that the "half-maximum temperature" (T_{50}), where Kim, et al.²¹ found NCRIf to decrease to half of the maximum at lowest temperatures, smoothly extends the dependence of T_{ip} on x_3 found here.

The same results as shown in Fig. 3 are replotted in Fig. 5 by normalizing the inverse temperature as T^{-1}/T_{ip}^{-1} and the dissipation as $\Delta Q_i^{-1}/\Delta Q_i(T_{ip})^{-1}$. Plotting in this manner reveals similarity and dissimilarity among the samples with varying ^3He impurity concentration. The normalized dissipation for the first mode in the 12 and 25 ppm samples and the second mode in the 25 ppm sample deviate considerably from others. The "sharp" increases in the normalized dissipation at high temperatures, $T_{ip}/T \lesssim 0.2$ (first mode) and 0.4 (second mode), become accentuated in Fig. 5. Deviations in the samples with higher x_3 from the other bell-shaped dependence on T_{ip}/T indicate an emergence of nearly temperature independent "extra" dissipation.

Annealing of solid ^4He samples has been found^{7,9,29} to affect the frequency shift and dissipation in TO experiments. Possible effects of sample "annealing" were studied in our $x_3 = 0.3 \text{ ppm}$ sample by raising the temperature of the cell up to 1.8 K (below the melting temperature of the sample) and maintaining the temperature for 10 hours. The temperature is then reduced to 0.3 K over six hours. Subsequently measured temperature dependence of the frequency shifts of the two modes are similar to those shown in Fig. 2 except f_{is}^0 decreases by 7.2 and 21.5 mHz for $i = 1$ and 2 , respectively. This observation is contrary to that of the recent experiment²⁹ which finds that the measured frequency shift at lowest

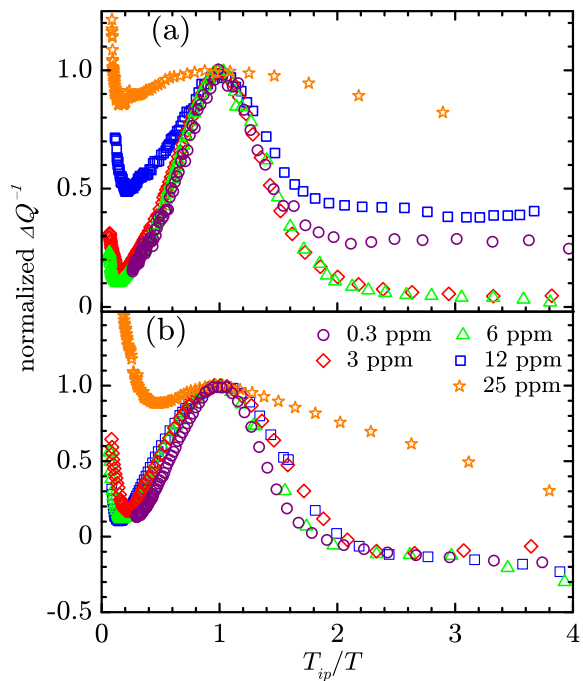


FIG. 5. (color online) Normalized (see text) change in dissipation: first mode (panel (a)) and second mode (panel (b)) of all samples shown in Fig. 3. Symbols: (purple) circles ($x_3[\text{ppm}] = 0.3$), (red) lozenges (3), (green) triangles (6), (blue) squares (12), and (orange) stars (25). Results shown for the 25 ppm sample include temperatures up to 2.5 K not displayed in Fig. 3.

temperatures is not affected by annealing. The dissipation peak temperatures decrease by about 5 mK after annealing. Our annealing process decreases the extracted (see Sec. IV) characteristic time slightly but produces no significant change in the activation energy.

IV. ANALYSIS

The original discovery¹ of frequency shifts at low temperatures in TOs loaded with solid ^4He and all subsequent confirmations, to our knowledge, have been accompanied by dissipations having puzzling resonance-like temperature dependence as exemplified by panel (a) in Fig. 3. In this section, we analyze the observed dependence of dissipations and frequency shifts on ^3He impurity concentration in solid ^4He samples. It is generally agreed that dissipation peaks occur at temperatures, where an internal dynamical rate (τ^{-1}) matches the imposed TO frequencies (ω_i), or where $\omega_i\tau = 1$. The internal dynamics of vortex motion³⁰, glassy response³¹, superglass^{11,32}, presence of tunneling two level systems³³, and viscoelastic behavior³⁴ have been suggested as the physical origin of dissipation. The vibration of dislocation line segments pinned at network nodes and by ^3He impurity has also been suggested³⁵ as the origin of the observed TO behavior.

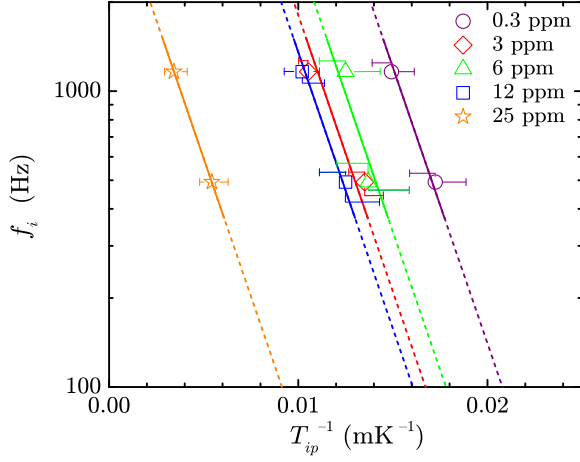


FIG. 6. (color online) Torsional oscillator frequencies plotted at inverse temperatures where dissipation peaks occur in solid ^4He samples with given ^3He impurity concentrations. All straight lines have the same slope corresponding to an activation energy E_0 of 430 mK and have ordinate intercepts which are adjusted for best fit for each sample. The intercepts represent the characteristic dynamic rate τ_0^{-1} (see text). Symbols for samples with different values of x_3 are same as those in Fig. 5.

Assuming that the internal dynamics is thermally driven, we consider a simple, activated dynamical time τ given by the Arrhenius form:

$$\tau = \tau_0 \exp \frac{E_0}{k_B(T - T_0)}, \quad (3)$$

where k_B is the Boltzmann constant, τ_0 a characteristic time and E_0 an activation energy. A possibly non-vanishing “transition temperature” T_0 is introduced in Eq. (3) for generality, but we assume $T_0 = 0$ in our analysis for simplicity. To examine our dissipation results in terms of Eq. (3), the mode frequencies are plotted in Fig. 4 on a logarithmic scale at corresponding T_{ip}^{-1} in each sample. The slopes and the intercepts determined strictly by straight lines (*not* shown) connecting the two points for each sample in Fig. 6 are $(E_0/k_B[\text{mK}], \tau_0^{-1}[\text{s}^{-1}]) = (380, 5 \times 10^{-7})$, $(290, 7 \times 10^{-6})$, $(720, 2 \times 10^{-8})$, $(370, 3 \times 10^{-6})$ and $(430, 3 \times 10^{-5})$ for $x_3 = 0.3, 3, 6, 12, 25$ ppm samples, respectively. Broadness in the dissipation peaks introduces considerable uncertainties (indicated by error bars in Fig. 6) in the values of T_{ip} and leads to scattering in these values of E_0/k_B and τ_0^{-1} . The tendency in Fig. 6, however, suggests that E_0 is a constant independent of x_3 . To make progress, let us assume that $E_0/k_B = 430$ mK, the average of above slopes, is a good estimate for the activation energy. It is interesting to note that this average activation energy is close to the binding energy of ^3He dislocation lines found in the analysis of their experiments by Kim, et al.²¹ and Day and Beamish.¹³

The intercepts of the best fits (shown by a straight line for each x_3 sample in Fig. 6) with the set slope specify

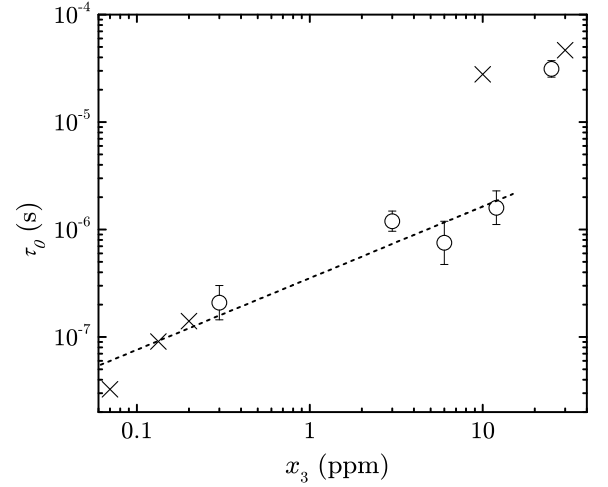


FIG. 7. Characteristic time τ_0 vs ^3He impurity concentration. The values of τ_0 are determined by the intercepts of the straight lines in Fig. 6. The dashed line represents $\tau_0 = 3.5 \times 10^{-7} x_3^{2/3}$ s (see Discussion section of text). Crosses show τ_0 calculated from the T_{50} data of Kim, et al.²¹ using the same activation energy as in Fig. 6 and their TO frequencies (see text).

the values of τ_0 as shown in Fig. 7. There is a trend for τ_0 to increase as x_3^γ where $\gamma \sim 2/3$ if $x_3 < 20$ ppm. Both the reduced frequency shifts and dissipation of 25 ppm sample show qualitatively different behaviors than the samples with lower ^3He impurity concentration. It appears that τ_0 also changes its dependence on x_3 beyond 20 ~ 25 ppm. It was already noted that the values of T_{50} measured by single frequency TO techniques by Kim, et al.²¹ are fairly close to T_{ip} (see Fig. 4). Constraining straight lines with the same slope as shown in Fig. 6 by their TO frequencies at T_{50}^{-1} imply values of τ_0 as shown in Fig. 7 for their samples. Considering differences in sample chamber geometry, sample growth process, measurement methods, etc., τ_0 extracted from T_{50} data of Kim, et al.²¹ overlaps and fits surprisingly well with extrapolation of our results to lower values of x_3 . Clearly it is of interest to extend frequency dependence studies like ours to smaller ^3He impurity concentration than we have carried out.

The mechanical response of driven TOs containing solid ^4He samples has been treated³¹ by including a general form of rotational susceptibility to account for the sample motion:

$$\chi = \frac{2G}{1 - (j\omega_i\tau)^\beta}, \quad (4)$$

where G is a constant (possibly dependent on frequency³⁶), ω_i is angular frequency, τ is a relaxation time, and β is an exponent dependent on a particular model. Including the general susceptibility results in extra dissipations and concomitant frequency shifts in the TO response. In our simplified analysis, the “Debye

model” response is considered by assuming $\beta = 1$. In this case, the change in dissipation due to sample motion is given by:

$$\Delta Q_i^{-1} = \frac{2G\omega_i\tau}{(1 + \omega_i^2\tau^2)}, \quad (5)$$

and the accompanying reduced frequency shift by:

$$\frac{f_{is} - f_{ib} - \Delta f_i}{f_{is}^0} = -\frac{G}{(1 + \omega_i^2\tau^2)} \quad (6)$$

Although the linear response model assumed here may not be entirely applicable to our experiment, it is of interest to examine if the model can achieve a similar success as in the description³⁷ of the shear modulus measurements. Our results are compared with those expected from Eq. (5) by assuming the Arrhenius form of relaxation time characterized by our average activation energy and the extracted τ_0 as shown in Fig. 7. Dissipations extracted from the experiment and from the model are compared in Fig. 8 for the 0.3 ppm sample. The observed peak dissipation of the first mode at T_{1p} is significantly larger than that of the second mode at T_{2p} in disagreement with the frequency independent peak dissipation expected from Eq. (5). To proceed with the (modified) Debye model, the value of G is *adjusted for each mode* separately to match the peak dissipation at T_{ip} in Fig. 8. Dissipations expected from the model produce narrower widths in temperature dependence around the peaks than those observed. Comparisons in other samples show similar deviations between the observations and the model. The model of course does not account for the upturns in dissipation at high temperatures nor for the low temperature residual dissipations observed in 12 and 25 ppm samples.

As seen in Fig. 8, the observed temperature dependence of dissipation is broader than than expected from the Debye model assuming Arrhenius relaxation time with one activation energy for the system. Broader temperature dependence may be introduced into the model by allowing a distribution in the activation energy. A canonical Gaussian distribution $N(E)$ given by

$$N(E) = \frac{1}{\sqrt{2\pi}w^2} e^{-\frac{1}{2}(\frac{E-E_0}{w})^2} \quad (7)$$

is applied to Eq. (5) to evaluate $\Delta\bar{Q}_i^{-1}$:

$$\Delta\bar{Q}_i^{-1}(T) = \int \Delta Q_i^{-1}(T, E) N(E) dE. \quad (8)$$

Here, E_0/k_B is set as the average activation energy and the width w of the distribution is adjusted for each sample. The peak dissipation value G is readjusted *separately* for each mode to match the respective peak dissipation. For the 3 ppm sample, adjusting to $w/k_B = 120$ mK can represent the data fairly well as shown in Fig. 8. In the cases of 12 and 25 ppm samples, there appear residual amounts of dissipation at low temperature. In these

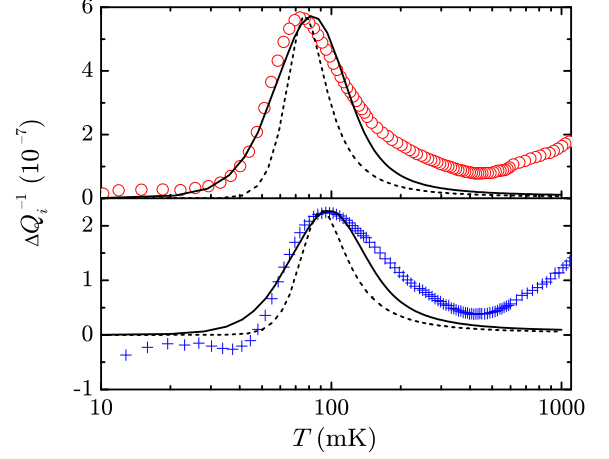


FIG. 8. (Color online) Comparison of dissipation in the 3 ppm sample with the dissipation expected from Debye susceptibility. Same data as shown in Fig. 3 are repeated for mode 1 ((red) circles) and 2 ((blue) pluses) in panel (a) and (b), respectively. In each panel, curves are dissipations expected (see text) from Eq. (5): assuming single activation energy and $\tau_0 = 1.2 \times 10^{-6}$ s and from Eq. (7) (dashed curves), and allowing Gaussian distribution of activation energy with $w/k_B = 120$ mK and from Eq. (8) (solid curves).

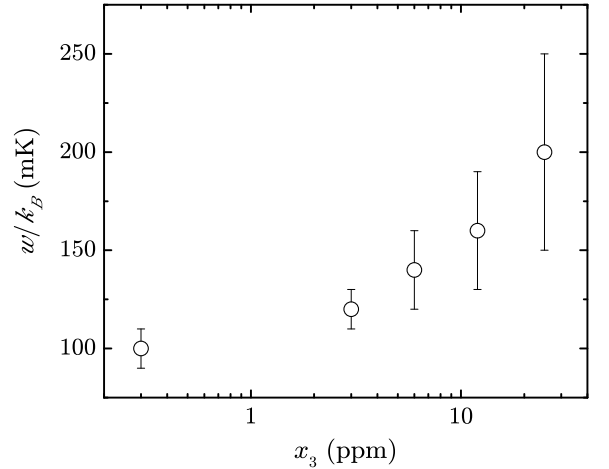


FIG. 9. Variation of width in distribution of activation energy. Widths are determined by fitting temperature dependence of dissipation in each sample using Eq. (7) and (8) (see text).

two samples, a constant added to ΔQ_i^{-1} is taken as an additional fitting parameter. The width of distribution obtained from fitting the data in this manner is shown in Fig. 9. Values of w within the error bars shown in Fig. 9 give similar goodness of fit for both modes. Despite large uncertainties, a clear increasing trend in w is discernable as x_3 is increased. We suggest that temperature widths around the dissipation peaks in TO experiments can provide sample characterization in the distribution of activation energy.

Using the same respective parameter values in eval-

uating dissipation for each mode shown in Fig. 8, the frequency shifts expected from Eq. (6), with single and distributed activation energy, are shown in Fig. 10 for the 3 ppm sample. The expected frequency shift of the first mode by including distribution in the activation energy approaches the observed frequency shift but a considerable difference remains. The expected frequency shifts of the second mode are much smaller than the observed. The large discrepancy in the second mode occurs despite independently adjusting the value of G for this mode as described above. The observed decrease in dissipation *and* increase in reduced frequency shift as the TO frequency is increased is a major inconsistency with the modified Debye model above. The difference in reduced frequency shifts between the measured and the Debye model would be a consequence of a superfluidity in solid ^4He . A similar conclusion is made by Yoo and Dorsey³⁴ in the analysis of their viscoelastic model for solid ^4He .

Despite the clear distinction demonstrated in the reduced frequency shifts between the measured and the modified Debye model, similarity in temperature dependence between the two in Fig. 10 is evident. Multiplying the Debye expectations shown by solid curves for the first and second mode by constants, 1.7 and 6.0, respectively, gives temperature dependence shown by dash-dotted curves in Fig. 10. Except in high temperature tail regions, the scaled temperature dependence matches the measured reduced frequency shifts quite well. Similar matching is seen in other samples with multiplicative constants applied to (first mode, second mode) of (1.4, 3.5), (1.3, 3.9), and (1.25, 3.6) in 0.3, 6 and 12 ppm samples, respectively. The 25 ppm sample cannot be matched in a similar manner owing to the large offset in dissipation. How this similarity in temperature dependence is related to the interpretation of supersolidity is not yet clear to us.

Nussinov, et al.³¹ and Graf, et al.³⁸ have carried out much more sophisticated analyses of observed TO responses with generalized rotational susceptibilities expressing glassy response. They found that various single frequency TO responses in both dissipation and frequency shift could be fitted by appropriately adjusting parameters in the glassy response model. Graf, et al.³⁹ recently reported their study of the frequency dependence in the dissipation and frequency shifts observed¹⁰ in our compound TO with a cylindrical sample chamber by allowing frequency dependence in the parameter G in Eq. (4). In our simple analysis of the observed ^3He impurity concentration dependent effects in the present annular sample chamber, we restricted ourselves to the above modified Debye model in which the value of G is *adjusted for each mode separately* to account for its apparent frequency dependence. Comparison of the cylindrical and annular sample chamber results indicates that the magnitude of *frequency dependence* of reduced frequency shifts increases as the sample chamber size is decreased.

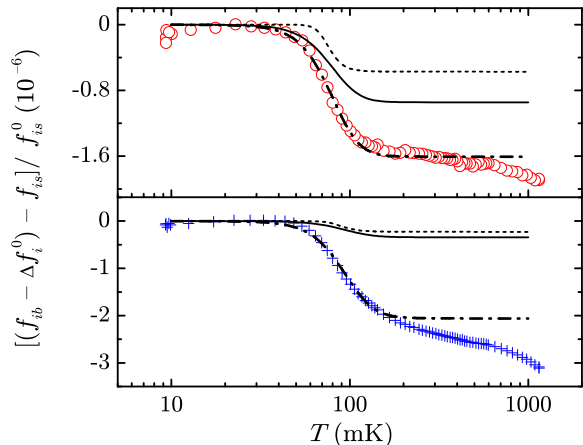


FIG. 10. (color online) Comparison of $x_3 = 3$ ppm sample frequency shift data with those expected from Debye susceptibility using parameters determined from fitting the dissipation data as shown in Fig. 8. Dashed and solid curves are those expected from the dissipations shown in Fig. 8 with the single activation energy and with the distribution of activation energy, respectively. Dash-dotted curves are obtained by multiplying the solid curves of the respective modes by constants (see text). Same data (but depopulated for clarity) as shown in Fig. 2 are repeated for mode 1 ((red) circles) and 2 ((blue) pluses) in panel (a) and (b), respectively.

V. DISCUSSION

It is noted that the extracted characteristic time shown in Fig. 7 varies almost in proportion to $x^{2/3}$ except for the 25 ppm sample. We speculate that this dependence stems from the diffusion process of ^3He condensed onto dislocation lines in solid ^4He samples. The diffusion time τ_d of ^3He along the dislocation lines may be approximated as $\tau_d \approx s^2/D$, where s is some characteristic distance over which ^3He moves during a time interval ω_i^{-1} , and $D \approx lv$ is a diffusion constant with mean free path l and particle velocity v . Let us suppose that the mean free path is approximately given by the effective dislocation loop length L . We follow Iwasa⁴⁰ in writing L as a parallel combination of the ^3He impurity length L_i and the network pinning length L_N :

$$L^{-1} = L_i^{-1} + L_N^{-1} \quad (9)$$

$$= \left[g x_3^{-\frac{2}{3}} \exp\left(-\frac{2W_0}{3T}\right) \right]^{-1} + L_N^{-1}, \quad (10)$$

where $g = 3.4 \times 10^{-7}$ (see Iwasa³⁵) is a constant and W_0 is the binding energy of ^3He impurity to dislocation line. At low temperatures where L_i dominates over L_N , the characteristic time takes on the Arrhenius form:

$$\tau_d = \frac{s^2}{gv} x_3^{\frac{2}{3}} \exp(E_0/T) \quad (11)$$

Identifying τ_d as τ and the coefficient on the right hand side of Eq. (11) as τ_0 , we expect it to depend on the

impurity concentration as $\propto x_3^{2/3}$. Letting $s^2/v = 1.2 \times 10^{-9}$ cm s, $W_0/k_B (= 3E_0/2k_B) = 0.65$ K, $L_N = 2$ μ m (similar "fits" can be achieved for $1 \sim 5$ μ m) gives the dependence on x_3 as shown by the dashed line in Fig. 7. This dependence appears to describe the observed dependence of τ_0 on x_3 except for the 25 ppm sample.

There are questions that can be raised on the above diffusion process to describe the observed characteristic time τ_0 as x_3 is varied. If the mean free path of a ^3He atom along a dislocation line is determined by other ^3He atoms condensed onto the dislocation line, it implies that ^4He atoms along the line mysteriously manage not to contribute to scattering. The process also implies that the diffusion coefficient of ^3He would *decrease* in the low temperature limit as $\exp(-E_0/T)$. This temperature dependence is in contrast to the temperature independent quantum diffusion coefficient of ^3He in bulk solid ^4He found by NMR experiments⁴¹ above 0.55 K. The Kyoto group has observed very long spin-lattice relaxation in their NMR experiment on solid ^4He sample with $x_3 \approx 30$ ppm. The long relaxation time might be related to the decreasing D implied by our analysis.

Iwasa³⁵ has analyzed TO experiments and shear modulus shifts in terms of the Granato-Lücke model⁴² on the interaction between an externally oscillated TO container and the induced vibrational motion of the dislocation lines present in the loaded ^4He solid sample. The analysis predicts shifting temperature dependence of the TO frequency and the dissipation peak temperature to higher temperatures as x_3 is increased in general agreement with observations. However, since the expected natural vibration frequencies of the dislocation lines are much higher than the TO frequencies so far attempted, little frequency dependence is expected in both frequency shift and dissipation. This aspect of the model³⁵ is yet to be reconciled with our TO experiments.

Gaudio, et al.⁴³ proposed a model⁴⁴ on the effects of ^3He on TO experiments where uniformly distributed ^3He impurities set the maximum grain size in solid ^4He samples. This model is not likely to be applicable in the range of values of x_3 in our experiments where ^3He atoms are expected to condense onto dislocation lines. Manousakis⁴⁵ considered ^3He impurity atoms binding to defects and promoting ^4He atoms to interstitial sites. It is not clear to us how this effect relates to the temperature dependent changes in dissipation observed here as x_3 is varied.

Day and Beamish¹³ discovered that temperature dependent changes in the shear modulus of solid ^4He were almost identical to those in frequency shifts observed in TO experiments. The discovery gives strong impetus for concluding that the observed changes in shear modulus and frequency shift have similar physical origin. Syshchenko, et al.³⁷ recently reported on their measurements of the changes in shear modulus and associated dissipation at frequencies between 0.5 Hz and 8 kHz.

They analyze (see also Su, et al.⁴⁶) their data with a Debye relaxation process and thermally activated dynamics just as we do. When a distribution of activation energy is included, they find that the relationship between the shear modulus and the dissipation can be accounted for at different frequencies by the assumed Debye and thermal activation processes. This is in sharp contrast to the analysis of our TO data: including distributions in activation energy cannot account for both frequency shifts and dissipations. The discrepancy increases at higher frequency (see Fig. 10).

VI. CONCLUSION

Effects of adding ^3He impurity to solid ^4He samples contained in an annular chamber were studied simultaneously at two resonant mode frequencies (differing by a factor of 2.4) by means of a compound torsional oscillator. Both frequency shifts and extra dissipations produced by the loaded samples were measured. Maxima in the measured dissipation occurred at impurity-concentration (x_3) dependent "peak temperatures" around which the frequency shifts varied more rapidly. When normalized to both the temperature and the dissipation level at the peak, the temperature dependence of dissipation became nearly universal in all samples studied except in the 25 ppm sample. A thermal activation energy (430 mK) and characteristic relaxation times were extracted from Arrhenius plots of frequency versus the inverse of dissipation peak temperature. The characteristic time increased with impurity concentration approximately as $x_3^{2/3}$ and suggested diffusion of ^3He atoms along dislocation lines as the dynamical process producing the observed dissipation. Observed temperature dependence of dissipation of both modes could be fairly well described by a simple Debye model by allowing for Gaussian distribution of activation energy *if* the magnitude of dissipation at the peak temperature was allowed to be frequency dependent. The measured magnitudes of frequency shifts were significantly greater than those expected from the model especially in the higher frequency mode. There remained "excess" amounts of frequency shifts which could not be accounted for by the simple Debye model. The excess frequency shifts may be attributed to superfluidity in solid ^4He at low temperatures. We believe that these frequency dependent effects hold a key to understanding of the dynamics of quantum solid ^4He .

VII. ACKNOWLEDGMENT

We thank Moses Chan for stimulating discussions. This research was supported by NSF DMR-0704120 and DMR-1005325.

-
- * Present address: Institute for Quantum Computing, University of Waterloo, ON, Canada.
- ¹ E. Kim and M. H. W. Chan, *Nature*(London), **427**, 225 (2004); *Science*, **305**, 1941 (2004).
 - ² N. Prokof'ev, *Adv. Phys.*, **56**, 381 (2007).
 - ³ S. Balibar and F. Caupin, *J. Phys. Cond. Mat.*, **20**, 173201 (2008).
 - ⁴ D. E. Galli and L. Reatto, *Journal of the Physical Society of Japan*, **77**, 1010 (2008).
 - ⁵ A. J. Leggett, *Phys. Rev. Lett.*, **25**, 1543 (1970).
 - ⁶ M. W. Meisel, *Physica B*, **178**, 121 (1992).
 - ⁷ A. S. C. Rittner and J. D. Reppy, *Phys. Rev. Lett.*, **97**, 165301 (2006).
 - ⁸ M. Kondo, S. Takada, Y. Shibayama, and K. Shirahama, *J. Low Temp. Phys.*, **148**, 695 (2007).
 - ⁹ A. Penzev, Y. Yasuta, and M. Kubota, *J. Low Temp. Phys.*, **148**, 677 (2007).
 - ¹⁰ Y. Aoki, J. C. Graves, and H. Kojima, *Phys. Rev. Lett.*, **99**, 015301 (2007).
 - ¹¹ B. Hunt, E. Pratt, V. Gadagkar, M. Yamashita, A. V. Balatsky, and J. C. Davis, *Science*, **324**, 632 (2009).
 - ¹² D. S. Greywall, *Phys. Rev. B*, **16**, 1291 (1977).
 - ¹³ J. Day and J. Beamish, *Nature*(London), **450**, 853 (2007).
 - ¹⁴ A. S. C. Rittner, W. Choi, E. J. Mueller, and J. D. Reppy, *Phys. Rev. B*, **80**, 224516 (2009).
 - ¹⁵ M. W. Ray and R. B. Hallock, *Phys. Rev. Lett.*, **100**, 235301 (2008).
 - ¹⁶ M. W. Ray and R. B. Hallock, *Phys. Rev. Lett.*, **105**, 145301 (2010).
 - ¹⁷ A. F. Andreev and I. M. Lifshitz, *Sov. Phys. JETP*, **29**, 1107 (1969).
 - ¹⁸ M. R. Sears and W. M. Saslow, *Phys. Rev. B*, **82**, 094519 (2010).
 - ¹⁹ Y. Aoki, H. Kojima, and X. Lin, *Low Temp. Phys.*, **34**, 329 (2008).
 - ²⁰ S. Kwon, N. Mulders, and E. Kim, *J. Low Temp. Phys.*, **158**, 590 (2010).
 - ²¹ E. Kim, J. S. Xia, J. T. West, X. Lin, A. C. Clark, and M. H. W. Chan, *Phys. Rev. Lett.*, **100**, 065301 (2008).
 - ²² R. Toda, P. Gumann, K. Kosaka, M. Kanemoto, W. Onoe, and Y. Sasaki, *Phys. Rev. B*, **81**, 214515 (2010).
 - ²³ R. Toda, W. Onoe, M. Kanemoto, T. Kakuda, Y. Tanaka, and Y. Sasaki, *J. Low Temp. Phys.*, **162**, 476 (2011).
 - ²⁴ S. S. Kim, C. Huan, L. Yin, J. Xia, D. Candela, and N. S. Sullivan, *J. Low Temp. Phys.*, **158**, 584 (2010).
 - ²⁵ S. S. Kim, C. Huan, L. Yin, J. Xia, D. Candela, and N. S. Sullivan, *ArXiv e-prints/10123709*.
 - ²⁶ Y. Aoki, J. Graves, and H. Kojima, *J. Low Temp. Phys.*, **150**, 252 (2008).
 - ²⁷ Emerson and Cuming, Billerica, MA 01821.
 - ²⁸ M. C. Keiderling, P. Gumann, D. Ruffner, and H. Kojima, To be published.
 - ²⁹ J. D. Reppy, *Phys. Rev. Lett.*, **104**, 255301 (2010).
 - ³⁰ P. W. Anderson, *Nat. Phys.*, **3**, 160 (2007); see also S. I. Shevchenko, *Sov. J. Low Temp. Phys.*, **13**, 61 (1987).
 - ³¹ Z. Nussinov, A. V. Balatsky, M. J. Graf, and S. A. Trugman, *Phys. Rev. B*, **76**, 014530 (2007).
 - ³² G. Biroli, C. Chamon, and F. Zamponi, *Phys. Rev. B*, **78**, 224306 (2008).
 - ³³ A. F. Andreev, *JETP*, **109**, 103 (2009).
 - ³⁴ C. D. Yoo and A. T. Dorsey, *Phys. Rev. B*, **79**, 100504 (2009).
 - ³⁵ I. Iwasa, *Phys. Rev. B*, **81**, 104527 (2010).
 - ³⁶ M. Graf, Z. Nussinov, and A. Balatsky, *J. Low Temp. Phys.*, **158**, 550 (2010).
 - ³⁷ O. Syshchenko, J. Day, and J. Beamish, *Phys. Rev. Lett.*, **104**, 195301 (2010).
 - ³⁸ M. J. Graf, A. V. Balatsky, Z. Nussinov, I. Grigorenko, and S. A. Trugman, *J. Phys. Conf. Series*, **150**, 032025 (2009).
 - ³⁹ M. Graf, J.-J. Su, H. Dahal, I. Grigorenko, and Z. Nussinov, *J. Low Temp. Phys.*, **162**, 500 (2011).
 - ⁴⁰ I. Iwasa and H. Suzuki, *J. Phys. Soc. Jpn*, **49**, 1722 (1980).
 - ⁴¹ A. R. Allen, M. G. Richards, and J. Schratte, *J. Low Temp. Phys.*, **47**, 289 (1982).
 - ⁴² A. Granato and K. Lücke, *J. App. Phys.*, **27**, 583 (1956).
 - ⁴³ S. Gaudio, E. Cappelluti, G. Rastelli, and L. Pietronero, *Phys. Rev. Lett.*, **101**, 075301 (2008).
 - ⁴⁴ B. Yucelsoy, J. Machta, N. Prokofev, and B. Svistunov, *Phys. Rev. Lett.*, **104**, 049601 (2010); S. Gaudio, E. Cappelluti, G. Rastelli, and L. Pietronero, *ibid.*, **104**, 049602 (2010).
 - ⁴⁵ E. Manousakis, *Europhysics Letters*, **78**, 36002 (2007).
 - ⁴⁶ J.-J. Su, M. J. Graf, and A. V. Balatsky, *Phys. Rev. Lett.*, **105**, 045302 (2010).